Control Allocation for Maneuver and Gust Load Alleviation of Flexible Aircraft

John H. Hansen*, Molong Duan†, Ilya V. Kolmanovsky‡, and Carlos E. S. Cesnik§
University of Michigan, Ann Arbor, Michigan, 48109, USA

As aircraft designs aim for higher aerodynamic efficiency, the structures become more flexible, requiring additional features to alleviate the loads encountered from gusts and maneuvers. With the additional feature of alleviating loads, it is preferable to minimize the change to the original flight trajectory tracking performance of the aircraft by exploiting redundant control effectors. In this work, a dynamic control allocation method for maneuver and gust load alleviation is proposed for flexible aircraft. The control architecture decouples the two objectives of load alleviation and rigid body trajectory tracking by exploiting the null space between the input and the rigid body output. A reduced-dimension null space variable is established and is optimally used to control the flexible output within user-defined bounds. A receding horizon approach is proposed to account for stochastic gust disturbances and maneuvers with limited preview. The proposed method is demonstrated through numerical simulations on a linearized model of the University of Michigan X-HALE aircraft.

Nomenclature

Δu	=	control input increment
Φ	=	power spectral density
σ_w	=	root mean square gust velocity
Ω	=	spatial frequency
B_g	=	gust influence matrix
B_u	=	control effector matrix
$C(s)$	=	nominal controller
g	=	gust signal
$G(s)$	=	model of flexible aircraft
$G_{fg}(s)$	=	model of flexible output due to gust
$G_{fu}(s)$	=	model of flexible output due to control input
$G_{rg}(s)$	=	model of rigid body output due to gust
$G_{ru}(s)$	=	model of rigid body output due to control input
$H(s)$	=	closed loop system
$\mathbf{H}$	=	closed loop system Toeplitz matrix
L	=	load alleviation block
L_t	=	turbulence length
k	=	iteration index for receding horizon approach
n_x	=	dimension of argument in subscript
$N(s)$	=	null space filter
r	=	reference signal
t	=	time
T_i	=	implementation interval
T_p	=	preview horizon
T_{man}	=	maneuver time
u	=	control input signal

*Major, U.S. Air Force, Ph.D. Candidate, Department of Aerospace Engineering, AIAA Student Member.
†Research Fellow, Department of Aerospace Engineering.
‡Professor, Department of Aerospace Engineering, AIAA Member.
§Professor, Department of Aerospace Engineering, AIAA Fellow.

u_0 = nominal control input
U_0 = peak gust velocity amplitude
v = null space variable
$\mathbf{v}$ = vector of sampled null space variable
x = internal state
y_f = flexible output
y_f^+ = upper bound on flexible output
y_f^- = lower bound on flexible output
y_r = rigid body output
$\mathbf{y}$ = vector of sampled output

I. Introduction

As aircraft are designed for increased fuel efficiency, high aspect ratio wings and lightweight structures emerge as key features. However, these key features often result in increased structural flexibility. A key challenge arising from increased flexibility is structural yielding or failure when the aircraft encounters aggressive flight maneuvers or gusts. Methods to alleviate the maneuver and gust loads on aircraft have been developed that are referred to as maneuver load alleviation (MLA) and gust load alleviation (GLA). While load alleviation helps to preserve the structural integrity, another objective is to maintain the aircraft maneuvering performance and trajectory tracking. Adverse effects on the maneuvering performance may lead to poor handling qualities or even affect how well the aircraft can complete its mission.

Several methods for load alleviation have been proposed using both hardware and software. Guo et al. [1] proposed a design for a passive gust load alleviation device at the wing tip. Fonte et al. [2] proposed a wing tip device for active control of loads due to maneuvers and gusts. Urnes et al. [3] proposed a variable camber flap control system installed along almost the entire span of the wing to control loads through all phases of flight. Including such hardware solutions in the design phase is preferred, instead of the sustainment phase of an aircraft life cycle. Adding new hardware to existing aircraft requires structural redesign, additional manufacturing and testing, which may come at high cost. Therefore, software solutions exploiting the existing control effectors are also appealing.

Early software methods of MLA systems symmetrically deflected the wing control surfaces (e.g., ailerons, flaps) based on aircraft normal acceleration to reduce structural loads [4]. An MLA efficiency study by Yang et al. [5] found that the efficient deflection is down for inboard control surfaces and up for outboard ones. This moves the wing load toward the fuselage of a conventional transport aircraft, reducing the bending moment at the root of the wing. Similar to MLA, GLA also uses the control surfaces to reduce the load, but it may not lead to symmetric deflections. Also, GLA typically requires a faster response to unanticipated dynamic loads [6]. Yagil et al. [7] used a two-step approach to gust alleviation by first constraining wing deformation of a highly flexible aircraft to within linear limits in steady trimmed flight while also allowing sufficient control margin for the second step using $\mathcal{H}_\infty$ loop shaping for the control of the dynamic response to gusts. More recently, light detection and ranging (LIDAR) devices have been proposed to forecast the gust [8]. In this scenario, it is assumed that a desired maneuver trajectory and the gust profile for the near future can be known a priori, therefore a unified load alleviation (LA) solution for both maneuver and gust loads is possible. The above proposed methods either allow or ignore the effects of the load alleviation system on the flight trajectory tracking. Therefore, an alternate approach for handling multiple objectives is desirable.

One enabling characteristic for LA is that the aircraft has more control inputs than the number of rigid body degrees of freedom, which are controlled to follow specific trajectories. This redundancy is referred to as over-actuation, and allows the control inputs to be optimally arranged to handle multiple objectives using control allocation techniques. The control allocation structure is usually comprised of two stages: The first stage is a high-level controller which guarantees the desirable output (e.g., flight trajectory tracking), while the second stage is a detailed allocator satisfying a secondary objective (e.g., load alleviation) [9]. Control allocation literature categorizes the dynamic system's input redundancy as either strong or weak. A system has strong input redundancy when it is possible to inject an arbitrary signal in certain input directions without affecting the state response of the plant. A system has weak input redundancy when the arbitrary signal does not affect the steady-state output of the system [10]. Strong input redundancy can also be thought of as when the number of control inputs exceeds the number of internal states used to define the system dynamics. Likewise, for weak input redundancy, the number of control inputs exceeds the number of controlled outputs. A review of relevant sources applying control allocation to MLA is included in the author's previous publication on the

subject [11]. However, these methods do not explicitly exploit the structure of input redundancy to decouple the two objectives of load alleviation and trajectory tracking, thus still introducing the tradeoff between them.

In this work, a dynamic control allocation method for unified load alleviation is proposed for weakly input redundant flexible aircraft. This work provides an expansion of the capability first described in [11], which only addressed MLA. This method augments the nominal control system of the aircraft and exploits the aircraft's redundant control effectors. The control architecture decouples the two objectives of load alleviation and rigid body trajectory tracking by exploiting the null space between the reference input and the rigid body output. A receding horizon approach is proposed to account for stochastic gust disturbances and maneuvers with limited preview. The proposed method is demonstrated through numerical simulations on a linearized model of a stiffened X-HALE aircraft [12] (shown in Fig. 1).

Fig. 1 X-HALE aircraft developed at University of Michigan

II. Modeling of Flexible Aircraft and Gust

A. Flexible Aircraft Modeling

1. Flexible Aircraft Model

Consider a flexible aircraft with n_u control inputs, including all control surfaces and thrusters. Assume the spatial dimension of the aircraft is relatively small compared to the gust ($< 10\%$), the gust is thus considered to be constant along the wingspan [13] and is represented by disturbances from longitudinal, lateral, and vertical directions, i.e., $g \in \mathbb{R}^3$. The gust is assumed to be known a priori over a given preview horizon T_p, which may be shorter than the total maneuver time T_{man}. As was described in [11], the outputs of the system include n_r rigid body outputs y_r (e.g., roll, pitch, yaw angles and their rates), and n_f flexible outputs y_f, which reflect structural deformation (e.g., curvature, bending moment, or load factor). It is assumed that there are more individual control input variables than rigid body outputs ($n_u > n_r$). The aircraft is initially in straight, level, unaccelerated flight, and its dynamics near this flight condition are represented by a linear time-invariant (LTI) model with state-space representation,

$$\begin{cases} \dot{x}(t) = Ax(t) + B_u u(t) + B_g g(t), \\ y_r(t) = C_r x(t), \\ y_f(t) = C_f x(t). \end{cases} \tag{1}$$

The internal state $x \in \mathbb{R}^{n_x}$ of this system is comprised of the rigid and flexible states of the aircraft. The system is assumed to be strictly proper (i.e., there are no feed through terms from input to output). Transfer function matrices are also used to represent this LTI system, i.e.,

$$\begin{bmatrix} y_f(s) \\ y_r(s) \end{bmatrix} = \underbrace{\begin{bmatrix} G_{fu}(s) & G_{fg}(s) \\ G_{ru}(s) & G_{rg}(s) \end{bmatrix}}_{G(s)} \begin{bmatrix} u(s) \\ g(s) \end{bmatrix}. \tag{2}$$

Here, $G_{fu}(s)$ and $G_{fg}(s)$ describe the dynamics of the flexible output of $G(s)$ from control inputs $u(s)$ and gust inputs $g(s)$, respectively. Likewise, $G_{ru}(s)$ and $G_{rg}(s)$ describe the dynamics of the rigid output of $G(s)$ from $u(s)$ and $g(s)$, respectively.

2. Input Redundancy in Flexible Aircraft

Input redundancy can be either strong or weak. For a system with strong input redundancy [10] the control effector matrix B_u in Eq. (1) has a nontrivial null space, i.e.,

$$Ker\,(B_u) \neq 0. \tag{3}$$

In flexible aircraft, the inclusion of the structural dynamics usually results in more states than control inputs, and Eq. (3) is not satisfied. In such a case, the notion of weak input redundancy [10, 14, 15] with respect to rigid body outputs can be used. Weak input redundancy with respect to rigid body outputs holds if

$$Ker\,(G_{ru}\,(j\omega)) \neq 0, \text{ for all } \omega. \tag{4}$$

In flexible aircraft with weak input redundancy a desired rigid body output trajectory can be realized by multiple different selections of control input trajectories. However, the various input trajectory selections may result in different trajectories for the flexible outputs. Consequently, weak input redundancy is exploited to achieve the two objectives of maintaining desired trajectory tracking by rigid body outputs while alleviating loads caused by maneuvers and gusts.

B. Gust Model

There are two general ways to model wind gusts: discrete and continuous. The influence of the gust on the aircraft model is prescribed by the gust influence matrix B_g, as in Eq. (1). For a gust assumed to come from only one direction, B_g matrix would have a single column. For a gust coming from any direction B_g has three columns corresponding to longitudinal, lateral, and vertical gust components.

1. Discrete Gust Model

The discrete gust model treats the gust as a deterministic disturbance to the system with finite temporal distribution [16]. A typical example of a discrete gust is represented by the 1−cosine profile disturbance to aircraft velocity. In the time domain, the discrete gust model is given by

$$g(t) = \frac{U_0}{2}\left[1 - \cos\left(\frac{2\pi t}{t_{\text{gust}}}\right)\right] \tag{5}$$

where the peak gust velocity amplitude is U_0 and the duration of the gust cycle is t_{gust}, while $t \in [0, T_{\text{man}}]$ is the time variable. The resultant signal defines the amplitude of the gust disturbance and is used as an input $g(t)$ in Eqs. (1) and (2).

2. Continuous Gust Model

For a continuous gust model, the gust velocity is modeled as a stochastic process with a known power spectral density (PSD) [16]. Two commonly used continuous gust models are the Dryden model and the von Karman model. The gust velocity PSD for the vertical and lateral directions of the Dryden model [17] is given by

$$\Phi(\Omega) = \sigma_w^2 \frac{L_t}{\pi}\left[\frac{1 + 3L_t^2\Omega^2}{(1 + L_t^2\Omega^2)^2}\right] \tag{6}$$

while the gust velocity PSD for the von Karman model is given by

$$\Phi(\Omega) = \sigma_w^2 \frac{L_t}{\pi} \left[\frac{1 + \frac{8}{3}(1.339 L_t \Omega)^2}{\left[1 + (1.339 L_t \Omega)^2\right]^{11/6}} \right]. \tag{7}$$

For each of these functions, σ_w is the root mean square gust velocity, L_t is the turbulence length, and Ω is the spatial frequency. Between these two models, the von Karman model gives a better fit to observed data and is the standard model used for commercial aircraft development. However, the Dryden model is mathematically convenient as it admits a low order realization. A time history of the gust velocity is generated by applying Gaussian white-noise as an input to the Dryden or von Karman model [17]. This time history is then used as as input $g(t)$ in Eqs. (1) and (2). MATLAB and Simulink have functions that generate Dryden or von Karman gust disturbances depending on aircraft velocity, altitude, and the direction cosines matrix.

III. Method

The load alleviation through control allocation system is depicted in the block diagram in Fig. 2. This paper enhances the methods in [11] with GLA capability and receding horizon implementation. In this control and load alleviation system, the rigid body output y_r is fed back to the nominal controller C to track a specified reference command $r(t) \in \mathbb{R}^{n_r}, 0 \le t \le T_{\text{man}}$. The controller generates a n_u-dimensional control input u_0 which, when applied to the flexible aircraft, produces the desired rigid output trajectory $y_r(t)$ (note that the nominal controller C directly generates control effector commands and hence it is different from typical flight controllers [18, 19], which generate required forces and moments but the proposed methodology can easily be extended to cover this case). These dynamics are occurring in the presence of gust disturbance . The combination of reference command and gust disturbance $g(t) \in \mathbb{R}^3$ from longitudinal, vertical, and lateral directions affects the rigid output trajectory, which is controlled by the nominal controller, and the flexible output y_f, which is not used in the nominal controller.

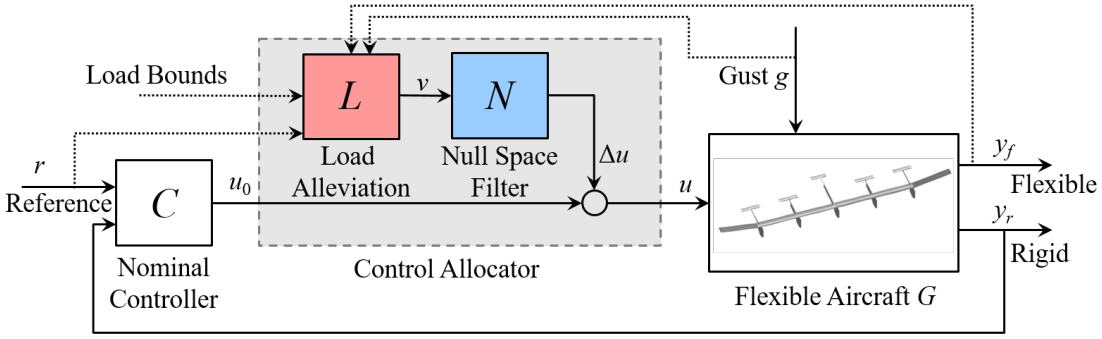

Fig. 2 Block diagram of load alleviation through control allocation

The weak input redundancy holds when the dimension of the control input n_u exceeds the dimension of the reference command n_r and Eq. (4) is satisfied. This weak input redundancy is exploited to control the flexible output. The process of controlling the flexible output is divided into two functions: (i) load alleviation calculation L and (ii) the null space filter N. The load alleviation calculation considers the reference signal $r(t)$, $0 \le t \le T_{\text{man}}$, a preview of the gust disturbance $g(t)$ over a limited horizon T_p, a model of the flexible aircraft with the nominal controller, and the load bounds and generates a trajectory for a null space variable $v(t)$ to ensure $y_f(t)$, $0 \le t \le T_{\text{man}}$ remains within the given bounds. The null space filter is a system that converts the null space variable v into a signal Δu (i.e., $\Delta u = N(s)v$), which is added to the control input u_0 from the nominal controller. The null space filter is designed so that its output signal Δu does not affect the rigid output y_r, thus enabling a decoupled implementation of load alleviation and trajectory tracking.

A. Null Space Filter Design

The null space filter is designed using the approach presented in [11, 20]. The design procedure relies on partitioning control signals into principal and redundant channels and exploiting matrix fraction description. The null space filter ensures that

$$G_{ru}(s)\Delta u(s) = 0 \tag{8}$$

irrespective of v. This is done by determining the level of input redundancy (i.e., $n_e = n_u - n_r$) and reorganizing the $G_{ru}(s)$ system according to n_r principal control inputs u_p and n_e extra control inputs u_e, i.e.,

$$G_{ru}(s) = \begin{bmatrix} G_p(s) & G_e(s) \end{bmatrix}, \; u = \begin{bmatrix} u_p^{\mathrm{T}} & u_e^{\mathrm{T}} \end{bmatrix}^{\mathrm{T}}. \tag{9}$$

Note that $G_p(s)$ is a square transfer function matrix that is also invertible and $G_e(s)$ is a $n_r \times n_e$ transfer function matrix. One way to generate a control increment Δu that achieves the desired effect in Eq. (8) is by defining a dynamic system, with an arbitrary n_e-dimensional signal v as its input, with the following form

$$\Delta u = \underbrace{\begin{bmatrix} G_p^{-1}(s)G_e(s) \\ -I \end{bmatrix}}_{N(s)} v. \tag{10}$$

The null space filter is then defined by Eq. (10) and additional details for using appropriate transformations to guarantee its stability are contained in [11, 20]. One can see that combining Eqs. (9) and (10) satisfies Eq. (8).

B. Determining Null Space Variable Trajectory by Quadratic Programming

To ensure that Δu affects y_f so that it lies within bounds y_f^- and y_f^+ for the entire maneuver time T_{man}, the condition on the null space variable v must first be derived. One difference between this work and the previous derivation in [11] is the inclusion of the gust disturbance. This process begins by analyzing the response of the rigid body output and flexible output, as functions of reference r, gust g, and null space variable v based on the following expressions:

$$\begin{aligned} &y_r(s) = G_{ru}(s)[u_0(s) + \Delta u(s)] + G_{rg}(s)g(s) = G_{ru}(s)C(s)[r(s) - y_r(s)] + G_{rg}(s)g(s) \Rightarrow \\ &y_r(s) = [I + G_{ru}(s)C(s)]^{-1}G_{ru}(s)C(s)r(s) + [I + G_{ru}(s)C(s)]^{-1}G_{rg}(s)g(s) \end{aligned} \tag{11}$$

$$\begin{aligned} &y_f(s) = G_{fu}(s)\left[u_0(s) + \Delta u(s)\right] + G_{fg}(s)g(s) \Rightarrow \\ &y_f(s) = G_{fu}(s)\left[C(s)\left(r(s) - y_r(s)\right) + N(s)v(s)\right] + G_{fg}(s)g(s) \end{aligned} \tag{12}$$

Inserting Eq. (11) into Eq. (12) yields

$$\begin{aligned} y_f(s) \;=\; & \underbrace{G_{fu}(s)C(s)\left[I - (I + G_{ru}(s)C(s))^{-1}G_{ru}(s)C(s)\right]}_{H_{fr}(s)} r(s) \\ & + \underbrace{\left[G_{fg}(s) - G_{fu}(s)C(s)(I + G_{ru}(s)C(s))^{-1}G_{rg}(s)\right]}_{H_{fg}(s)} g(s) + \underbrace{G_{fu}(s)N(s)}_{H_{fv}(s)} v(s), \end{aligned} \tag{13}$$

which is expressed as the following state space representation of the closed loop system:

$$\begin{aligned} \dot{x}_{\mathrm{CL}} &= A_{\mathrm{CL}}x_{\mathrm{CL}} + B_{r,\mathrm{CL}}r + B_{g,\mathrm{CL}}g + B_{v,\mathrm{CL}}v \\ y_f &= C_{f,\mathrm{CL}}x_{\mathrm{CL}}. \end{aligned} \tag{14}$$

Let $y_f(t)$, $t \geq 0$ denote the time-domain solution of the flexible output from Eq. (14) assuming zero initial conditions, i.e.,

$$y_f(t) = y_{fr}(t, r(t)) + y_{fg}(t, g(t)) + y_{fv}(t, v(t)), \tag{15}$$

where y_{fr} is the component of the flexible output from the reference signal, and y_{fg} and y_{fv} are similar components from the gust and null space signals, respectively. Setting Eq. (15) in relation to the load bounds yields the following constraints:

$$\begin{aligned} &y_f^- \leq y_f(t) \leq y_f^+ \Leftrightarrow \\ &y_{fv}(t, v(t)) \geq y_f^- - y_{fr}(t, r(t)) - y_{fg}(t, g(t)), \\ &y_{fv}(t, v(t)) \leq y_f^+ - y_{fr}(t, r(t)) - y_{fg}(t, g(t)). \end{aligned} \tag{16}$$

In order to find the optimal $v(t)$, the system is formulated as a quadratic programming problem where the objective function is the 2-norm of $v(t)$. A simulation of the flexible output response for T_{man} is calculated using the model of the flexible aircraft with nominal controller, along with assumed reference and gust inputs, with $v(t) = 0$. These results provide the components of the right hand side of the constraints in Eq. (16) and show where load bounds are violated. The solution of the quadratic programming problem provides the optimal $v(t)$ to control the flexible output within the load bounds, according to the dynamics of Eq. (14). When using a discrete-time format, filtering v with $H_{fv}(s)$ is represented by the multiplication of Toeplitz matrix $\mathbf{H}_{fv}$ and $\mathbf{v}$ (sampled $v(t)$ arranged in a single-column vector), as detailed in [11]. The flexible output components are also sampled and arranged in single-column vectors $\mathbf{y}_{fr}$ and $\mathbf{y}_{fg}$. Therefore, the system is formulated as the following quadratic programming problem:

$$\begin{aligned} \min_{\mathbf{v}} \quad & \mathbf{v}^{\mathrm{T}}\mathbf{v}, \\ \text{s.t.} \quad & \mathbf{H}_{fv}\mathbf{v} \leq y_f^+ - \mathbf{y}_{fr} - \mathbf{y}_{fg}, \\ & -\mathbf{H}_{fv}\mathbf{v} \leq -y_f^- + \mathbf{y}_{fr} + \mathbf{y}_{fg}. \end{aligned} \tag{17}$$

The above analysis assumes the initial conditions for all dynamics of the combined systems in Eq. (13) are equal to zero, which is reasonable since the systems are all based on linearized systems about a trim point, and the maneuver starts from this trim condition. Also note that this analysis assumes complete knowledge of the reference and gust inputs for the entire maneuver time a priori. This approach is henceforth referred to as the "full preview" approach. The assumptions used for this approach may not be realistic for maneuvers lasting longer than two to three seconds, especially when considering the stochastic nature of gust disturbances, therefore a more robust approach is desired for such circumstances.

C. Receding Horizon Implementation

The receding horizon approach intends to provide a more robust way to handle maneuvers lasting longer than a few seconds, and the stochastic nature of continuous gust disturbances. The approach assumes that the prior knowledge of reference and gust inputs have a limited preview horizon T_p (e.g., a few seconds). The solution for the null space variable v is calculated for the preview horizon, but only the first part of that solution is applied to the system (the shorter time interval is referred to as the implementation interval T_i). For example, the the k^{th} calculation interval spans $(k-1)T_i \leq t \leq (k-1)T_i + T_p$ and the solution from $(k-1)T_i$ to kT_i is implemented. In this way, the entire maneuver over T_{man} requires at least $\lceil T_{\text{man}}/T_i \rceil$ implementation intervals. This approach removes the assumption of zero initial conditions because the system is not in an equilibrium condition at the beginning of each implementation interval. Removing this assumption requires a modification to the analysis for calculating the optimal solution of the null space variable.

The system response at each implementation interval now varies with the initial condition of the internal state of the closed loop system in Eq. (14) at the implementation time (e.g., $x_{\text{CL}}(kT_i)$) and the input signals. In this way, Eq. (15) becomes

$$y_f(t) = y_{f_0}(t, x_{\text{CL}}(kT_i)) + y_{fr}(t, r(t)) + y_{fg}(t, g(t)) + y_{fv}(t, v(t)) \text{ for } kT_i \leq t \leq kT_i + T_p. \tag{18}$$

Therefore, the condition for the null space variable in Eq. (16) for the receding horizon approach becomes

$$\begin{aligned} & y_f^- \leq y_f(t) \leq y_f^+ \Leftrightarrow \\ & y_{fv}(t, v(t)) \geq y_f^- - y_{f_0}(t, x_{\text{CL}}(kT_i)) - y_{fr}(t, r(t)) - y_{fg}(t, g(t)), \\ & y_{fv}(t, v(t)) \leq y_f^+ - y_{f_0}(t, x_{\text{CL}}(kT_i)) - y_{fr}(t, r(t)) - y_{fg}(t, g(t)), \end{aligned} \tag{19}$$

for $kT_i \leq t \leq kT_i + T_p$. For each implementation interval, the initial condition of the internal state $x_{\text{CL}}(kT_i)$ is known for the upcoming preview horizon. The objective of the load alleviation block L is to determine the optimal trajectory for the null space variable $v(t)$ based on this inequality constraint.

As in the full preview approach, to find the optimal $v(t)$, the system is formulated as a quadratic programming problem (Eq. (17)). However, for the receding horizon approach, a computationally efficient solution is obtained when the objective function is the square of the 2-norm of the difference $\Delta v_k(t)$ relative to an assumed null space trajectory $v_{a,k}(t)$, i.e.,

$$v_k(t) = v_{a,k}(t) + \Delta v_k(t), \tag{20}$$

for $(k-1)T_i \le t \le (k-1)T_i + T_p$. A simulation of the flexible output response for the k^{th} preview horizon T_p is calculated using assumed reference, gust, and $v_{a,k}(t)$ inputs for $(k-1)T_i \le t \le (k-1)T_i + T_p$. For the first preview horizon, this simulation assumes $v_{a,1}(t) = 0$, $0 \le t \le T_p$. The $\Delta v_k(t)$ solution is found by the quadratic programming problem and then added to $v_{a,k}(t)$ to form $v_k(t)$ but only the value for the first implementation interval is applied to the system, while the rest of the $v_k(t)$ solution is used as $v_{a,k+1}(t)$ for the first $T_p - T_i$ portion of the next calculation interval. Due to the receding preview horizon, $v_{a,k+1}(t)$ over $(k-1)T_i + T_p \le t \le kT_i + T_p$ is assumed to linearly reduce to zero. The simulation of the flexible output response is then run for the $k+1$ preview horizon, using $v_{a,k+1}(t)$ and the corresponding assumed values for $r(t)$ and $g(t)$ for $kT_i \le t \le (kT_i + T_p)$. Therefore, in order to find the optimal $\Delta v_k(t)$ to control the flexible output for each implementation interval, the quadratic programming problem becomes:

$$\begin{aligned} \min_{\mathbf{\Delta v}_k} \quad & \mathbf{\Delta v}_k^{\mathrm{T}} \mathbf{\Delta v}_k, \\ \text{s.t.} \quad & \mathbf{H}_{fv} \mathbf{\Delta v}_k \le y_f^+ - \mathbf{y}_{f_0,k} - \mathbf{y}_{fr,k} - \mathbf{y}_{fg,k}, \\ & -\mathbf{H}_{fv} \mathbf{\Delta v}_k \le -y_f^- + \mathbf{y}_{f_0,k} + \mathbf{y}_{fr,k} + \mathbf{y}_{fg,k}, \end{aligned} \tag{21}$$

where $\mathbf{\Delta v}_k$, $\mathbf{y}_{f_0,k}$, $\mathbf{y}_{fr,k}$, and $\mathbf{y}_{fg,k}$ are the sampled single-column vectors of their time-domain counterparts over the k^{th} calculation interval. There is no guarantee of feasibility of Eq. (21), however, the constraints can be relaxed with slack variables to ensure feasibility. The computational load for the quadratic programming problem increases with the number of redundant control effectors n_e and the chosen time duration of the preview horizon T_p. However, choosing a shorter T_p may results in an infeasible problem, depending on the structural dynamics of the flexible aircraft and the magnitude and rate of the load excursion. Another way to potentially reduce computational load is to represent v as basis functions with an appropriate transformation matrix.

IV. Simulation Case Studies

A. X-HALE Modeling and Nominal Control

The proposed method is demonstrated using a linearized model of the X-HALE aircraft [12]. As depicted in Fig. 3, the X-HALE has two roll spoilers, four elevators, and five thrusters, i.e., $n_u = 11$. The nominal controller for the aircraft model was developed in [11, 21] which includes decoupled, cascaded proportional/proportional-integral (P/PI) controllers for the roll and pitch rates, while a proportional controller is used for the yaw rate. The nominal controller stabilizes the rigid body output of roll, pitch, and yaw rates (i.e., $n_r = 3$) based on pilot input. By observation, the criterion for weak input redundancy given in Eq. (4) is satisfied because $n_u > n_r$. There are two critical flexible outputs to be controlled by the unified load alleviation scheme which are, specifically, the out-of-plane bending curvature values at the two inner-most wing sections S_{R1} and S_{L1} (see Fig. 3).

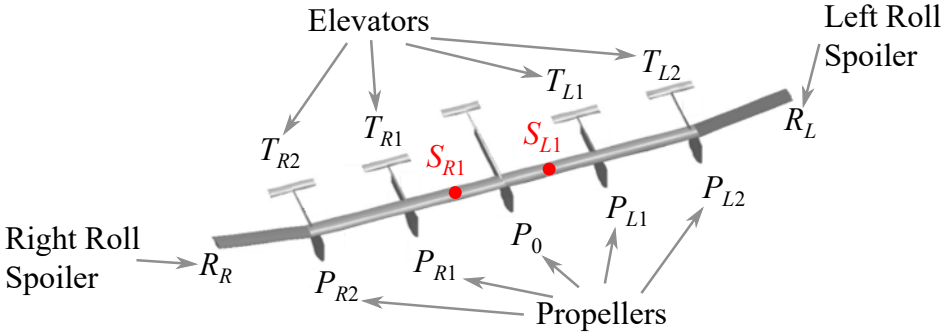

Fig. 3 Control inputs and critical stations on X-HALE [11]

The X-HALE was modeled and linearized using the University of Michigan Nonlinear Aeroelastic Simulation Toolbox (UM/NAST), which uses a strain-based formulation to model elastic and rigid-body dynamics of aerospace structures [22]. The stiffness of the X-HALE model was numerically doubled versus the real aircraft so that the linearized model represents flexible aircraft, rather than very flexible aircraft. This modification is consistent with the assumption of linear structural dynamics because the shape deformation is limited.

The linearized model was generated by first defining a trim point of straight, level, unaccelerated flight. A typical trim flight condition, with an airspeed of 14 m/s at an altitude of 30 m, was chosen to create the linearized model. At this flight condition, the aircraft wing has a baseline deformation at the two critical points S_{R1} and S_{L1}, whose out-of-plane curvatures equal -0.052 m^{-1}. Note that an upward bend is represented by a negative curvature value since it is negatively curved around the longitudinal axis. The curvature bounds for the load alleviation solver (Eq. (17)) were set to ± 0.056 m^{-1}. The proposed method was demonstrated by importing the linearized model of X-HALE into MATLAB and Simulink (ver. R2016a) to make all other calculations and produce simulation results.

B. Gust Model Implementation

A basic B_g matrix was generated by using the direction cosines matrix for the attitude of the aircraft center of gravity at the equilibrium condition to establish a connection between the body fixed frame of reference and the inertial frame of reference. The velocity of the wind gusts was then assumed to directly add to the rigid body velocity components at the center of gravity, as related through the direction cosines matrix. This influence of gust disturbances from longitudinal, vertical, and lateral directions were then captured in a B_g matrix for three gust disturbance components. By this assumption, the gust velocity directly impacts only the rigid body motion through the aircraft center of gravity. The effect of the gust disturbance on the flexible output results from the structural dynamics captured in the model. As a result, a downward gust increases the out-of-plane wing bending and an upward gust decreases bending. A more accurate way to account for the gust disturbances could be through the analysis of the aerodynamic influence on the lifting surfaces and control surfaces; such a treatment is left to future research.

The time signal for the discrete gust used for simulation was generated using Eq. (5). This gust was assumed to be in the downward vertical direction because it provides the most direct effect to increase wing bending for the assumptions made when generating the B_g matrix.

The continuous gust disturbance was implemented using the "Dryden Wind Turbulence Model" (Discrete, -q, +r) block in Simulink. The block parameters were set with a six meter wind of 5 m/s, from the north. The probability of exceedance of high-altitude intensity was "10^{-2} - Light" and the scale length was 762 meters, which is a standard value of 2,500 feet [17]. The wingspan was set to 6 meters and the sample time was 0.001 seconds. With these parameters, the block uses the current aircraft altitude, velocity, and direction cosines matrix based on the current attitude to generate longitudinal, lateral, and vertical velocity components of turbulence. These components were used as the inputs to the static B_g from Eq. (1) matrix which was defined at the equilibrium condition.

C. Simulation Results of Load Alleviation Demonstration for X-HALE

Four general test cases with increasing complexity (i.e., discrete gust, continuous gust, longitudinal maneuver with gust, and multi-axis maneuver with gust) were used for this demonstration.

(i) Discrete gust encounter: The aircraft encounters a discrete downward gust with a $1-$cosine profile. The gust is encountered two seconds after the simulation starts, swelling to a peak gust amplitude of $U_0 = 0.002$ m/s and then decaying to zero over two seconds (i.e., $t_{\text{gust}} = 2$ s). No maneuver is provided for this case, i.e., the controller aims to maintain straight and level flight.

(ii) Dryden turbulence encounter: The aircraft is flying in a turbulence field characterized by a Dryden model. No maneuver is provided for this case, i.e., the controller aims to maintain straight and level flight.

(iii) Descent with turbulence: The aircraft is descending to a lower altitude in the presence of turbulence characterized by the Dryden model. The reference trajectory consists of a pitch down two seconds after the simulation starts with a pulse of $-7.8^\circ/$s, intended to achieve -6° of pitch in one second (equilibrium condition pitch attitude is $+1.8^\circ$). The nose-down pitch attitude is held for four seconds before leveling off in one additional second. This maneuver results in a descent of 10 meters.

(iv) Descending turn with turbulence: The aircraft is descending while executing a right turn in the presence of turbulence characterized by the Dryden model. The reference trajectory initiates the turn one second after the simulation starts. A reference pulse of $30^\circ/$s is given for the roll rate and a reference yaw rate of $15^\circ/$s is established in one second. The bank angle and yaw rate are held for six seconds before the reference reverses the initial signal over one second to return to zero bank angle on a new heading. This results in a target heading angle change of 105°. The descent portion of the trajectory is the same as in the descent maneuver.

Test case (i) with discrete gust uses the full preview method discussed in Section III.B, while the other test cases use the receding horizon approach discussed in Section III.C. For the receding horizon approach, the preview horizon T_p was set to three seconds and implementation interval T_i was set to 0.1 seconds. The discrete-time linear models used a

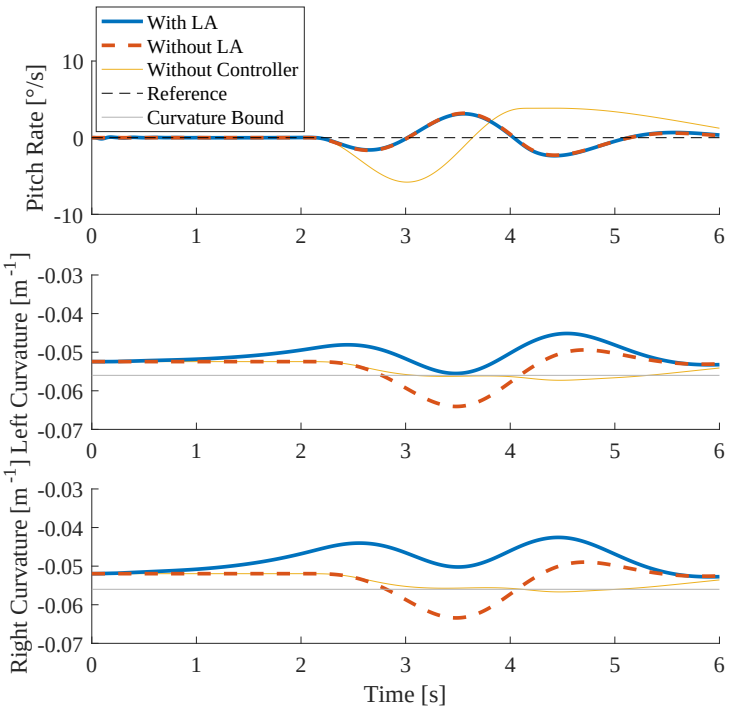

Fig. 4 Responses of pitch rate and wing root bending curvature for test case (i): discrete downward gust with and without LA

time step of 0.001 seconds. The quadratic programming problems in Eqs. (17) and (21) are solved using the "lsqlin" function in MATLAB, using the active-set algorithm.

The results for test case (i) are shown in Figs. 4 and 5. Figure 4 shows the pitch rate response and the out-of-plane bending curvatures at the critical stations while encountering the discrete gust. The yellow line shows the aircraft response without any flight controller. The X-HALE shows a stablizing response, but note that the structural loads (bending curvature) are not very high. Note that higher negative values indicate increased upward curvature. The aircraft response with the nominal controller engaged (red dashed line) shows a much faster return to the trim point, but results in higher loads. This shows that gust disturbances are not necessarily the cause of structural loads, but rather it is due to the flight controller or operator responding to the disturbance. The aircraft response with the load alleviation control allocator activated is shown by the solid blue line. Note that the pitch response with and without the LA are identical, indicating that the trajectory tracking performance is not affected by the LA method and the decoupled design is effective. The bending curvatures exceed the specified constraints without LA through control allocation and are kept within the bounds by using the proposed LA scheme.

The time histories of the tail and roll spoiler inputs for test case (i) are shown in Fig. 5. The incremental changes to the thruster inputs were less than one percent of the normalized throttle signal and, therefore, are not shown. To alleviate the load, the roll spoilers are engaged symmetrically to reduce the lift at the wing tips, while they were not used at all for the response without LA. The left and right outer tails increase the deflections which caused the high bending curvature without LA, which shows that more lifting load is being supported at the outer pods (at two-thirds of the length of the wing). The left and right inner tails deflect opposite of the response from the nominal controller, showing less load being supported at the inner pods (at one-third of the length of the wing). This result seems to contradict the conclusions presented by [5], which showed efficient deflections were down for inboard control surfaces and up for outboard control surfaces. However, note that the analysis in the literature was for conventional transport aircraft, where the majority of the mass is in the fuselage, attached to the roots of the wings. The X-HALE mass is distributed along its wingspan, therefore, a different result is understandable and insightful for this type of aircraft.

One can see that the control surfaces begin deflecting to reduce the bending curvature at around one second into the simulation. This is one second before the gust is encountered and around 1.75 seconds before the curvature bounds are

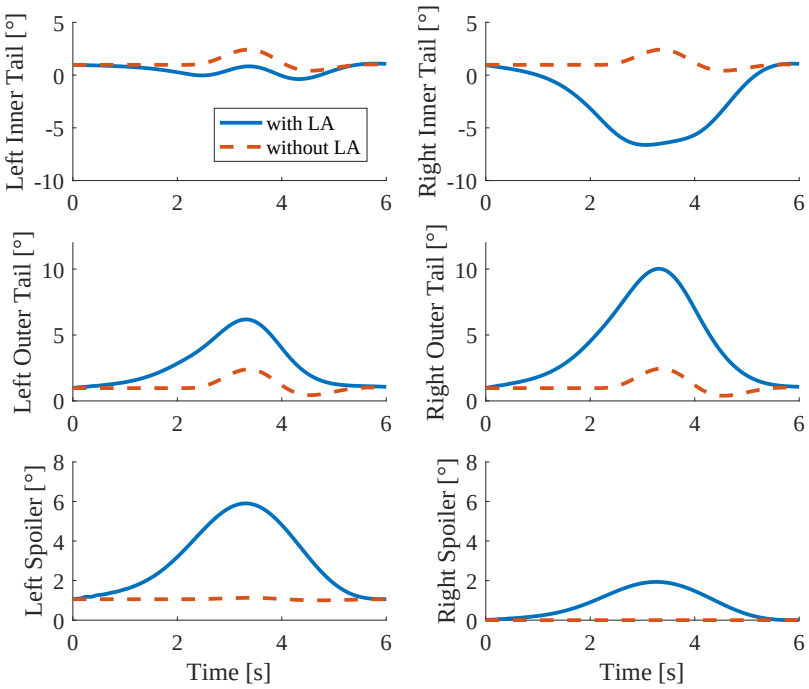

Fig. 5 Time histories of tail and roll spoiler inputs for test case (i): discrete downward gust with and without LA

exceeded without LA. This shows that the proposed method manipulates the structures in anticipation of a future load exceedance, due to the preview horizon and a priori knowledge of the gust and controller response.

The rigid body response and the bending curvatures at the critical stations while encountering turbulence in level flight for test case (ii) are shown in Fig. 6. The response with the nominal controller disengaged, is again presented by the yellow line, which results in higher curvature values, than the discrete gust. In this case, the nominal controller reduces the maximum bending curvature during the simulation, but still results in curvatures in excess of the bounds. As in the previous test case, the trajectory tracking performance is not affected by LA method and the bending curvatures are kept within the bounds by using the proposed LA scheme. The time histories of the tail and roll spoiler inputs are shown in Fig. 7. Note that the control surfaces are engaged before the prolonged bending curvature exceedance which begins at two seconds into the simulation in order keep the gust and controller response within the bounds. One can also see that the null space variable is not used for the last few seconds of the simulation since there is no exceedance of bounds to correct.

The rigid body response and the bending curvatures at the critical stations while descending in turbulence in test case (iii) are shown in Fig. 8. The command to pitch down alleviates some of the excess loads that were observed at this point in the simulation during case (ii). However, the command to pitch up when stopping the descent results in a large and abrupt excursion of the curvature bounds just before eight seconds into the simulation. Again, the trajectory tracking performance is not affected by LA method and the bending curvatures are kept within the bounds by using the proposed LA scheme. The time histories of the tail and roll spoiler inputs are shown in Fig. 9. The anticipatory nature of the LA system is observed again, as well as times in the middle and very end of the simulation, where the LA system is not engaged.

The rigid body response and the bending curvatures at the critical stations while executing a descending turn in turbulence in test case (iv) are shown in Fig. 10. The combination of the multi-axis maneuver and turbulence results in a prolonged exceedance of the bending curvature for over four seconds. The highest curvature occurs suddenly, just before the eight second mark, as the aircraft pitches back up to level flight while still turning. The amplitude and rate of this exceedance provided a good test case of the performance limits of the LA system. A shorter preview horizon T_p of

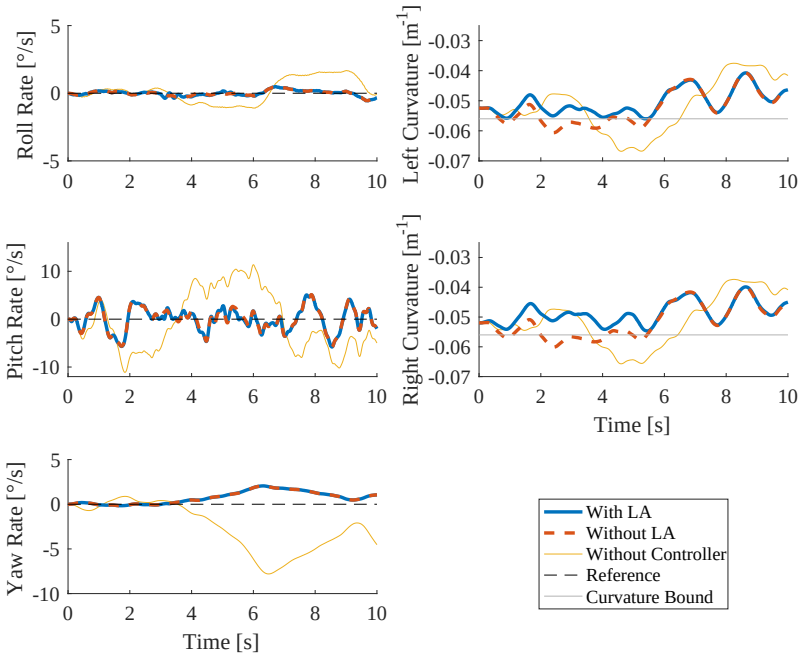

Fig. 6 Responses of rigid body motion and wing root bending curvature for test case (ii): turbulence with and without LA

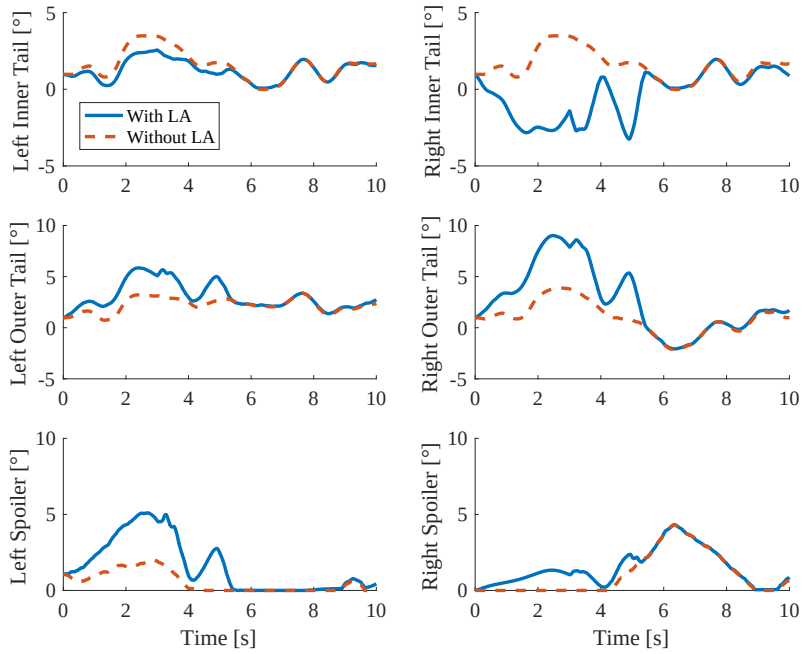

Fig. 7 Time histories of tail and roll spoiler inputs for test case (ii): turbulence with and without LA

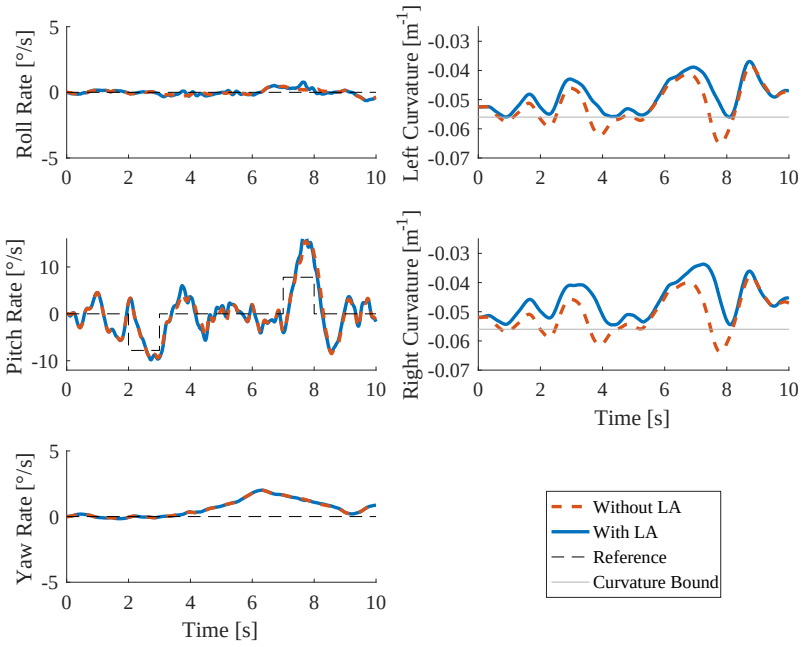

Fig. 8 Responses of rigid body motion and wing root bending curvature for test case (iii): descent in turbulence with and without LA

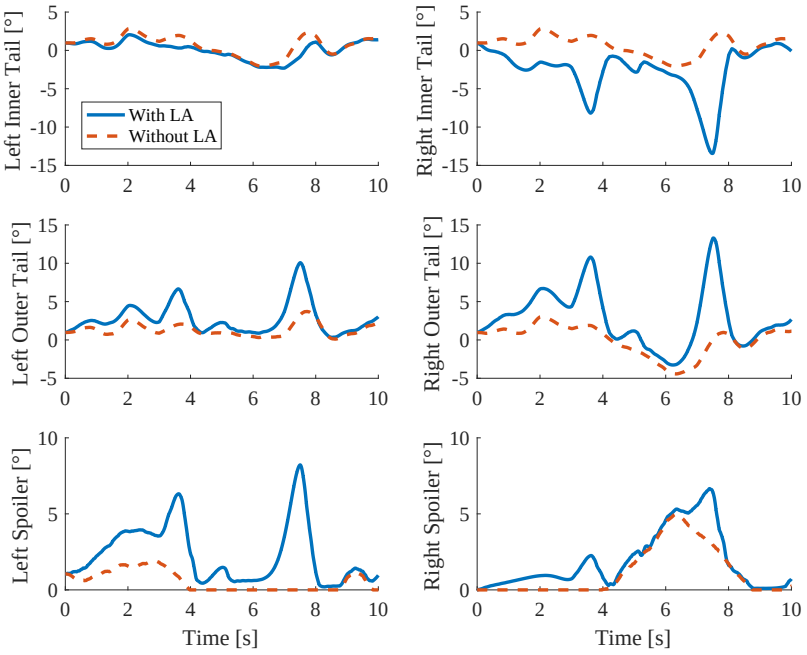

Fig. 9 Time histories of tail and roll spoiler inputs for test case (iii): descent in turbulence with and without LA

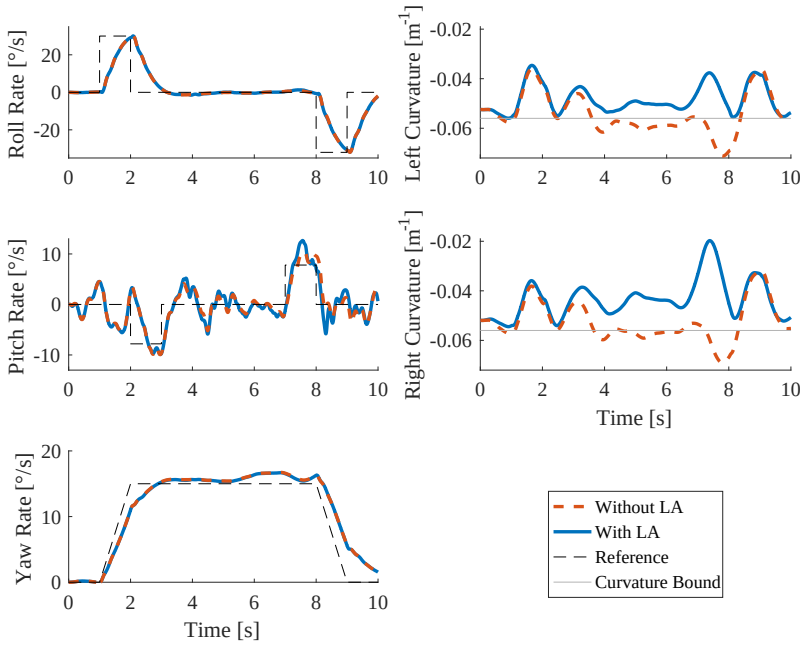

Fig. 10 Responses of rigid body motion and wing root bending curvature for test case (iv): descending turn in turbulence with and without LA

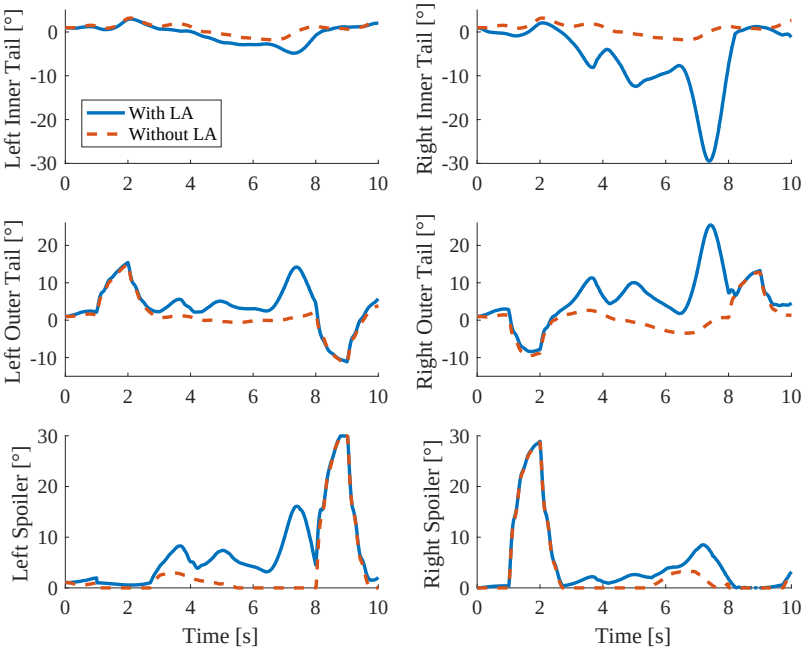

Fig. 11 Time histories of tail and roll spoiler inputs for test case (iv): descending turn in turbulence with and without LA

two seconds was used for this test case, but the solver for Eq. (21) could not find a feasible solution at this point in the simulation. This was corrected by increasing T_p to three seconds, which allowed for adequate anticipatory control input to manipulate the structure in such a way that the pitch up maneuver and turbulence did not exceed the bending curvature bounds. Around this time in the simulation, some high frequency differences in the pitch response are observed as well, which shows a limitation of the null space filter for large values of the null space variable. Aside from that instance, the trajectory tracking performance is not affected by LA method. The bending curvatures are kept within the bounds throughout the simulation time. The time histories of the tail and roll spoiler inputs are shown in Fig. 11. This test case resulted in the highest use of the control surfaces, both for the maneuver commands and for the load alleviation.

V. Conclusion

In this paper, a dynamic control allocation method for maneuver and gust load alleviation (LA) has been proposed for flexible aircraft. This LA method exploits the null space between the reference input and the rigid body output arising from redundant control effectors. By using the null space, the control architecture decouples the two objectives of load alleviation and rigid body trajectory tracking. A reduced-dimension null space variable is established, which only affects the flexible output when passed through a null space filter to generate incremental control signals. A receding horizon approach to optimize the trajectory of the null space variable has been proposed which reduces the loads at critical stations of the aircraft. Numerical simulations on a linearized model of the University of Michigan X-HALE aircraft show that the proposed LA method can successfully avoid the violation of load bounds resulting from both gust disturbances and maneuvers, and without affecting the trajectory tracking performance. Extensions of this approach to handle linear parameter varying and nonlinear systems are left to future research.

References

[1] Guo, S., Fu, Q., and Sensburg, O. K., "Optimal Design of a Passive Gust Alleviation Device for a Flying Wing Aircraft," *12th AIAA Aviation Technology, Integration, and Operations (ATIO) Conference and 14th AIAA/ISSM*, AIAA, Indianapolis, Indiana, 2012, p. 5625.

[2] Fonte, F., Toffol, F., and Ricci, S., "Design of a Wing Tip Device for Active Maneuver and Gust Load Alleviation," *2018 AIAA/ASCE/AHS/ASC Structures, Structural Dynamics, and Materials Conference*, 2018, p. 1442.

[3] Urnes, J., Nguyen, N., Ippolito, C., Totah, J., Trinh, K., and Ting, E., "A Mission Adaptive Variable Camber Flap Control System to Optimize High Lift and Cruise Lift to Drag Ratios of Future N+3 Transport Aircraft," *51st AIAA Aerospace Sciences Meeting including the New Horizons Forum and Aerospace Exposition*, 2013, p. 214.

[4] White, R. J., "Improving the Airplane Efficiency by Use of Wing Maneuver Load Alleviation," *Journal of Aircraft*, Vol. 8, No. 10, 1971, pp. 769–775.

[5] Yang, Y., Wu, Z., and Yang, C., "Control Surface Efficiency Analysis and Utilization of an Elastic Airplane for Maneuver Loads Alleviation," *54th AIAA/ASME/ASCE/AHS/ASC Structures, Structural Dynamics, and Materials Conference*, 2013, pp. 1–7.

[6] Xu, J., and Kroo, I., "Aircraft Design with Active Load Alleviation and Natural Laminar Flow," *Journal of Aircraft*, Vol. 51, No. 5, 2014, pp. 1532–1545.

[7] Yagil, L., Raveh, D. E., and Idan, M., "Deformation Control of Highly Flexible Aircraft in Trimmed Flight and Gust Encounter," *Journal of Aircraft*, Vol. 55, No. 2, 2018, pp. 829–840.

[8] Kopf, M., Bullinger, E., Giesseler, H.-g., Adden, S., and Findeisen, R., "Model Predictive Control for Aircraft Load Alleviation: Opportunities and Challenges," *2018 Annual American Control Conference (ACC)*, Milwaukee, USA, 2018, pp. 2417–2424.

[9] Johansen, T. A., and Fossen, T. I., "Control Allocation—a Survey," *Automatica*, Vol. 49, No. 5, 2013, pp. 1087–1103.

[10] Zaccarian, L., "Dynamic Allocation for Input Redundant Control Systems," *Automatica*, Vol. 45, No. 6, 2009, pp. 1431–1438.

[11] Duan, M., Hansen, J. H., Kolmanovsky, I. V., and Cesnik, C. E. S., "Maneuver Load Alleviation of Flexible Aircraft through Control Allocation: A Case Study using X-HALE," *International Forum on Aeroelasticity and Structural Dynamics*, 2019, p. 109.

[12] Cesnik, C. E. S., Senatore, P. J., Su, W., Atkins, E. M., and Shearer, C. M., "X-HALE: A Very Flexible Unmanned Aerial Vehicle for Nonlinear Aeroelastic Tests," *AIAA journal*, Vol. 50, No. 12, 2012, pp. 2820–2833.

[13] Diederich, F. W., "Response of an Airplane to Random Atmospheric Disturbances," Tech. Rep. TN3910, NACA, April 1957.

[14] Duan, M., and Okwudire, C., "Proxy-Based Optimal Control Allocation for Dual-Input Over-Actuated Systems," *IEEE/ASME Transactions on Mechatronics*, Vol. 23, No. 2, 2018, pp. 895–905.

[15] Duan, M., and Okwudire, C. E., "Connections between Control Allocation and Linear Quadratic Control for Weakly Redundant Systems," *Automatica*, Vol. 101, 2019, pp. 96–102.

[16] Dillsaver, M. J., Cesnik, C. E. S., and Kolmanovsky, I. V., "Gust Load Alleviation Control for Very Flexible Aircraft," *AIAA Atmospheric Flight Mechanics Conference*, AIAA, Portland, Oregon, 2011, p. 6368.

[17] Hoblit, F. M., *Gust Loads on Aircraft: Concepts and Applications*, American Institute of Aeronautics and Astronautics, Inc., Washington, DC, 1988.

[18] Oppenheimer, M. W., Doman, D. B., and Bolender, M. A., "Control Allocation," *The Control Handbook*, edited by W. S. Levine, CRC Press, Boca Raton, 2010, Chap. 8, 2nd ed., pp. 8–24.

[19] Yildiz, Y., and Kolmanovsky, I., "Stability Properties and Cross-Coupling Performance of the Control Allocation Scheme CAPIO," *Journal of Guidance, Control, and Dynamics*, Vol. 34, No. 4, 2011, pp. 1190–1196.

[20] Duan, M., and Okwudire, C., "Proxy-Based Optimal Dynamic Control Allocation for Multi-Input, Multi-Output Over-Actuated Systems," *Proceedings of the ASME 2017 Dynamic Systems and Control Conference*, ASME, Tyson, VA, 2017, p. V001T03A005.

[21] Pang, Z. Y., "Modeling, Simulation and Control of Very Flexible Unmanned Aerial Vehicle," Ph.D. thesis, University of Michigan, Ann Arbor, 2018.

[22] Cesnik, C. E. S., and Su, W., "Nonlinear Aeroelastic Simulation of X-HALE: a Very Flexible UAV," *49th AIAA Aerospace Sciences Meeting Including the New Horizons Forum and Aerospace Exposition*, 2011, p. 1226.